Electronic Supplementary Material (ESI) for ChemComm.

Supporting Information

Light-induced desorption of trivalent chromium from adsorbents: one step closer to sustainability

Xiaoyu Guan[a], Sunxian Yan[a], Jinming Chang[a], Gaofu Yang[a], Haojun Fan[b*]

[a] *Key Laboratory of Leather Chemistry and Engineering of Ministry of Education, Sichuan University, Chengdu 610065, P.R. China*

[b] *National Engineering Laboratory for Clean Technology of Leather Manufacture, Sichuan University, Chengdu 610065, P.R. China*

* Corresponding author.

E-mail address: fanhaojun@scu.edu.cn

Contents

1. Materials

2,*3*,*3*-trimethylindolenine (≥ 98%), *3*-iodopropanoic acid (≥ 98%), *5*-nitrosalicylaldehyde (≥ 99%), and Si <100> wafer (10 × 10 × 0.6 mm^3) (SW) were purchased from Sigma-Aldrich (St. Louis, MO). (*3*-Aminopropyl) triethoxysilane (AMEO, ≥97.0%), *1*-ethyl-*3*-(*3*-dimethylaminepropyl) carbodiimide hydrochloride (EDC·HCl, ≥98.5%), *N*-hydroxysuccinimide (NHS, ≥98.0%), Ferric chloride hexahydrate ($FeCl_3 \cdot 6H_2O$, reagent grade, ≥ 98.0%), sodium acetate (NaAc, chemical grade), ethylene glycol (EG, ≥ 99.5%), and polyethylene glycol (PEG, M_n=1500) were purchased from Kelong Chemical Engineering Co. Ltd. (Chengdu, China). The metal chloride of sodium (Na^+), potassium (K^+), plumbum (Pb^{2+}), calcium (Ca^{2+}), chromium (Cr^{3+}), and ferric (Fe^{3+}) were all analytical grade supplied by Cheng Jie Chemical Engineering Co. Ltd. (Shanghai, China). Toluene, dichloromethane (DCM), ethanol, acetonitrile (TFA), and dimethylformamide (DMF) were dried over 4 sieves and distilled. Ultrapure water was Milli-Q grade (resistivity higher than 18.2 MΩ·cm at 25 ^oC) obtained from a Millipore Simplicity 185 system.

2. Experiment

2.1 Synthesis of spiropyran derivate containing a carboxyl (SP) [1]

2.5 g of *2*,*3*,*3*-Trimethylindolenine and 3.14 g of *3*-iodopropanoic acid were dissolved in 3 mL of toluene and heated under nitrogen in the dark at 100 °C for 3 h. After that, the resulting solution was cooled and evaporated to dryness. The residue was partitioned between water (50 mL) and chloroform (25 mL), and the aqueous layer was extracted with chloroform (2 × 25 mL). Finally, evaporation of water obtained the intermediate product (4.6 g, 83%). The intermediate product was characterized by FTIR (Figure S1), ^{1}H NMR (Figure S2), and ESI-MS (Figure S3).

1.01 g of the intermediate product and 0.47 g of 5-nitrosalicylaldehyde were dissolved in 10 mL of anhydrous ethanol and stirred for 10 min. Hereafter, 0.30 mL of piperidine was added at one time, and the mixture was refluxed under nitrogen in the dark at 80 °C for 5 h. The resultant was cooled in an ice bath and filtered, and the filter was further washed with cold ethanol three times. Finally, the precipitate was dried in vacuum to yield a spiropyran derivate containing a carboxyl (SP) (1.04 g, 70%) as a yellow powder. SP was characterized by FTIR (Figure S4), ^{1}H NMR (Figure S5), and ESI-MS (Figure S6). The synthesis procedure and the structure of SP were illustrated in Scheme S1.

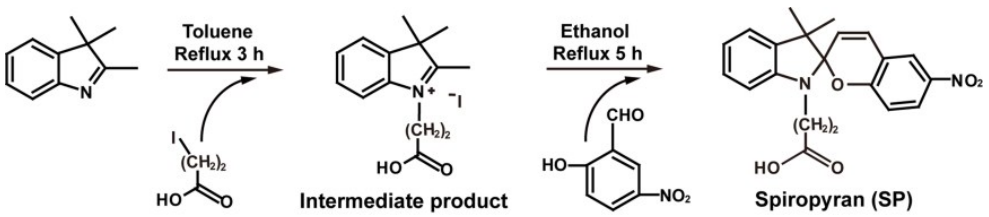

Scheme S1. Synthesis and structure of SP.

2.2 Preparation of SP@SW

The original silicon wafer (OSW) substrates were sonicate by using acetone, ethanol, and ultrapure water sequentially, 20 min for each process. Hereafter, the substrates were cleaned by treatment in a hot, freshly prepared piranha solution (H_2SO_4 (98%):H_2O_2 (30%) 3:1 v/v) for 30 min ***(Caution: piranha solution is extremely corrosive and should be handled only with the proper equipment)***. Then, the substrates were thoroughly washed with pure Milli-Q water and dried under a flow of ultrapure N_2, finally yielding the cleaned and plasma silicon wafers (SW).

Into a flame-dried reaction flask was placed a freshly cleaned SW, followed by dry toluene (10 mL) and 0.5 mL of AMEO. The reaction flask was then heated under N_2 at 90 °C for 20 h. Hereafter, the substrate was removed and washed repeatedly with toluene followed by acetone and dried under a flow of ultrapure N_2, yielding a amine-functionalized wafer (NH_2-SW).

To a solution of EDC·HCl (22.5 mg) and NHS (13.5 mg) in anhydrous DCM (10 mL) was added SP (42.7 mg) and NH_2-SW wafers were added into the stirred solution. The reaction mixture was cooled for the first hour at 5 °C and left to react at 10 °C for 8 h. The wafers were then exhaustively washed with DCM to remove any SP, EDC·HCl or NHS, dried under a flow of ultrapure N_2, and stored at room temperature. The finally product was defined as SP@SW. The synthesis procedure and the structure of SP@SW were illustrated in Scheme 1 (Main manuscript).

2.3 Preparation of SP@Fe_3O_4

Magnetite particles (Fe_3O_4) were synthesized through a solvothermal reduction method according to previous literature [2]. In briefly, 1.0 g of $FeCl_3·6H_2O$ was dissolved into 30 mL of EG to form a clear solution, and followed by addition of 2.7 g of NaAc and 0.75 g of PEG. The resulting mixture was stirred for 30 min, and then transferred to a Teflonlined stainless-steel autoclave for heating at 200 °C. After 8 h, the autoclave was allowed to cool to room temperature. The black products were

washed five times with ethanol and then vacuum-dried at 60 °C for 6 h.

For covalent immobilization of carboxyl-terminated spiropyran (SP), Fe_3O_4 was modified by AMEO first. Fe_3O_4 (0.5 mg) were added into toluene solution (15 mL), and ultrasonically oscillated for 10 min. Then, AMEO (0.1 mL) was added *via* the equivalently fractionated drop method under nitrogen atmosphere at 90 °C within 20 h. After that, the product, NH_2-Fe_3O_4, was washed five times with ethanol and vacuum-dried at 50 °C until a constant mass.

To a solution of EDC·HCl (1.2 mg) and NHS (0.6 mg) in anhydrous dichloromethane (DCM, 10 mL) was added SP (1.98 mg), stirring the mixture for 30 min. Then, NH_2-Fe_3O_4 (4.0 mg) was added and then left to be cured at 10 °C under nitrogen protection for 8 h. After that, the obtained product, SP@Fe_3O_4, was washed with DCM to remove any SP, EDC·HCl or NHS and vacuum-dried at 50 °C for further use. The synthesis procedure and the structure of SP@Fe_3O_4 were illustrated in Scheme 1 (Main manuscript).

3. Characterization

^{1}H nuclear magnetic resonance (^{1}H NMR) spectra were recorded on a Bruker Ettlingen (Germany) AV600 NMR spectrometer in deuterated dimethyl sulfoxide (DMSO-*d*6) solution and the chemical shifts were determined relative to the residual solvent peak (δ_H 2.50 for DMSO). The following abbreviations are employed to indicate signal multiplicity: s, singlet; d, doublet; t, triplet; q, quartet; m, multiplet; dd, doublet of doublets. Electrospray ionization mass spectrometry (ESI-MS) was conducted on a Finnigan TSQ Quantum Ultra (America) instrument. High performance liquid chromatography (HPLC) was carried out with an Agilent binary pump system using a YMC-Pack Pro C18 column (150 × 20 mm; 5 μm particle size) fitted with a guard column. The eluents A and B are 0.1% TFA in acetonitrile and 0.1% aq. TFA, respectively. The sample was eluted with a flow rate of 0.5 mL/min. Ratios were determined at the isosbestic point λ = 360 nm. Fourier transform infrared (FTIR) spectra were recorded in transmission mode on a Nicolet iS10 FTIR spectrometer (Thermo Scientific, United States) in KBr plates over a wavenumber range from 400 to 4000 cm^{-1} after 64 scans at a resolution of 2 cm^{-1}. Furthermore, attenuated total reflectance-fourier transform infrared (ATR-FTIR) spectra were acquired with a Nicolet 6700 FTIR (Thermo Scientific, United States) spectrometer equipped with a mercury-cadmium-telluride detector cooled with liquid nitrogen. The diamond ATR accessory (Golden Gate™, Specac) was positioned in the sample compartment, connected to a dry air supply for purging and aligned for measurements. Measurements were performed at a spectral resolution of 4 cm^{-1} and 128 co-added scans were used for all measurements of the silicon wafer samples throughout this investigation. The silicon wafers were placed to cover the whole diamond (2 mm × 2 mm) ATR-crystal. The UV-Vis absorbance spectra recorded on a UV-3600 (Shimadzu, Japan) instrument equipped with an external thermostat (Neslab RTE digital circulating water bath) using a quartz cuvette of 10 mm path length. Excitation-emission fluorescence spectra were collected using a fluorimeter (Cary Eclipse, Varian, United States) equipped with a 1.0 cm quartz

cell. The morphology of the adsorbents were visualized by using a field-emission scanning electron microscopy (FE-SEM, JSM-7500F, JEOL, Japan) equipped with an energy-dispersive X-ray spectroscope (EDS, X-MAX50, JEOL, Japan) and a transmission electron microscopy (TEM, JEM-2010, JEOL, Japan) manipulated at an accelerating voltage of 200 kV. Atomic force microscope (AFM) was conducted on a SPM-9600 instrument (SHIMADZU, Japan) at room temperature to determine the surface features as a result of interactions between a scanning probe and the sample. Fluorescence microscopy imaging was carried out on a Zeiss Axioplan2 upright microscope and images were acquired using a Hamamatsu OrcaER cooled CCD camera with MetaMorph acquisition software when the slides were observed under a 100× oil immersion objective. Excitation-emission fluorescence spectra were collected using a fluorimeter (Cary Eclipse, Varian, United States) equipped with a 1.0 cm quartz cell. X-ray photoelectronic spectroscopy (XPS) was performed on an AXIS Ultra DLD instrument (Kratos, United Kingdom) with a monochromatic Al Kα X-ray as the excitation source (1486.6 eV). The concentration of residuary metal ions was determined by inductively coupled plasma-optical emission spectroscope (ICP-OES, Optima 2100 DV, Perkin-Elmer Instruments, United States). Visible light ($\lambda > 400$ nm) was generated by a flashlight-LED (R838, Warsun, Inc., China) with a power of 10 W. Irradiation distance was set about for 8 cm.

4. Results

4.1 Characterization of the intermediate product and SP

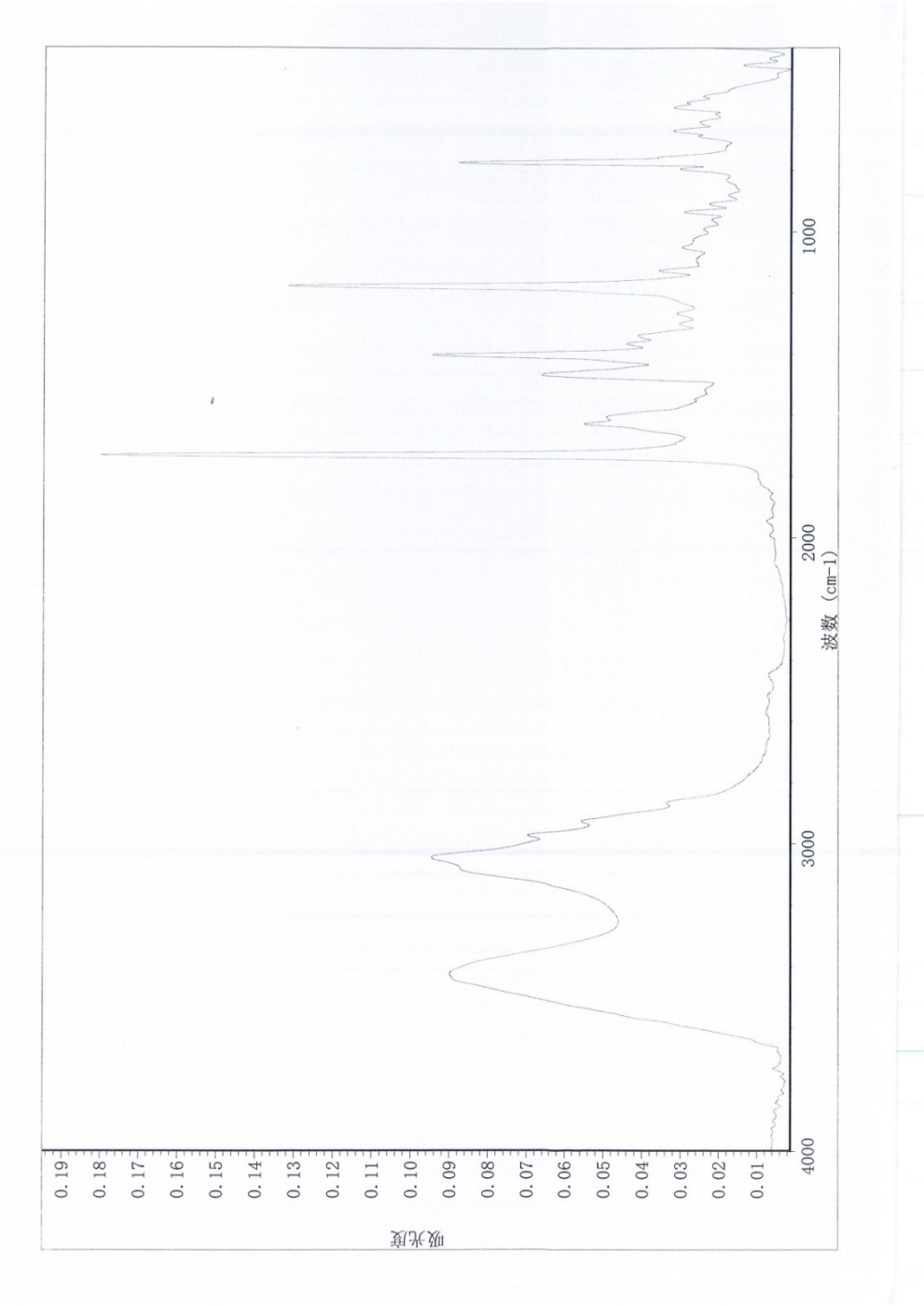

Figure S1. FTIR spectrum of intermediate product.

FTIR (4000-400, cm^{-1}): dominated absorbance peaks, 1728 cm^{-1} (υ_{COOH}), 1608 cm^{-1} ($\upsilon_{C=C}$).

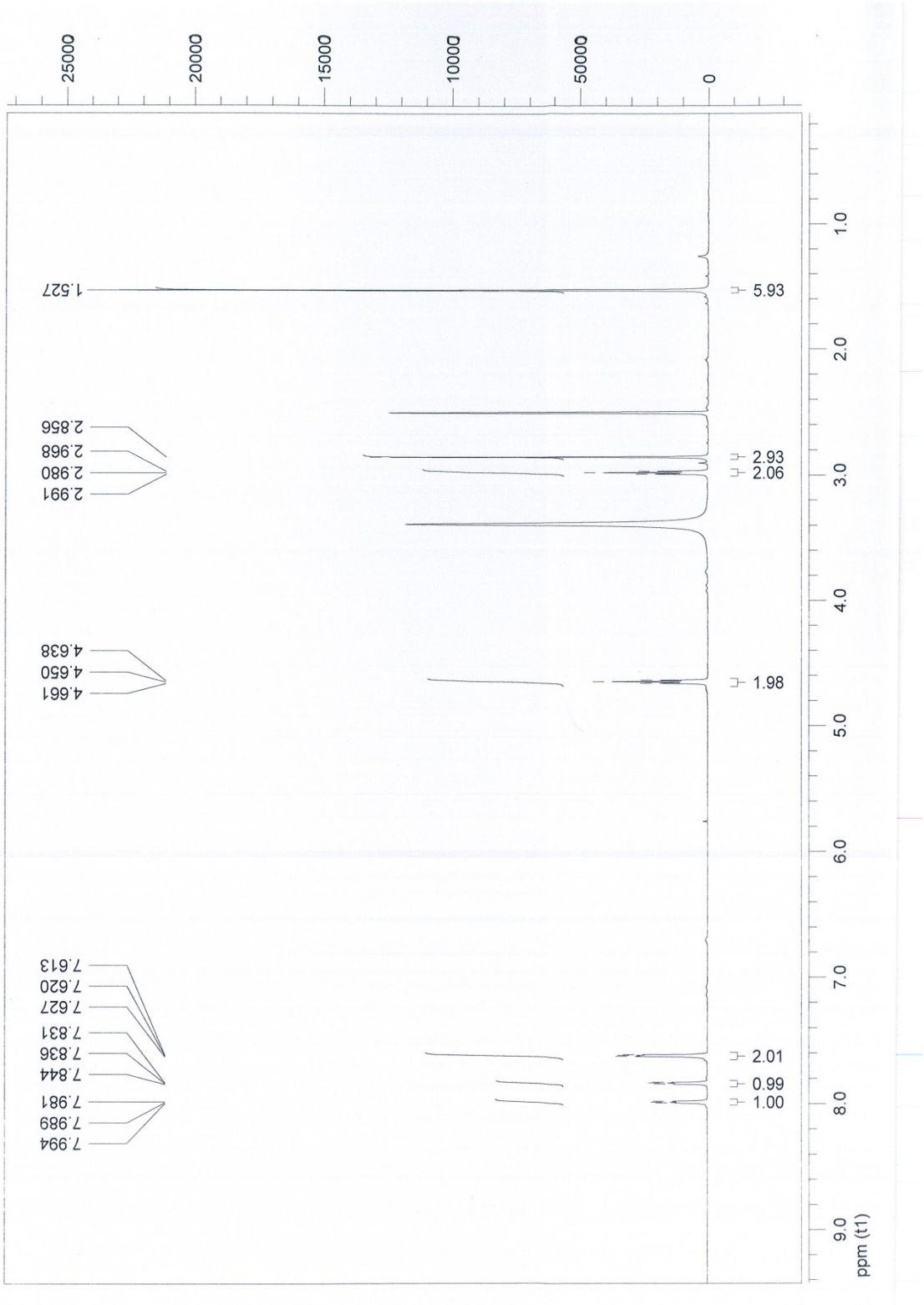

Figure S2. ^{1}H NMR spectrum of intermediate product.

^{1}H NMR (DMSO-d_6, 600 MHz): δ 1.52 (s, 6H), δ 2.85 (s, 3H), δ 2.96-2.99 (t, 2H), δ 4.63-4.66 (t, 2H), δ 7.61-7.63 (m, 2H), δ 7.82-7.84 (dd, 1H), δ7.97- 7.99 (dd, 1H).

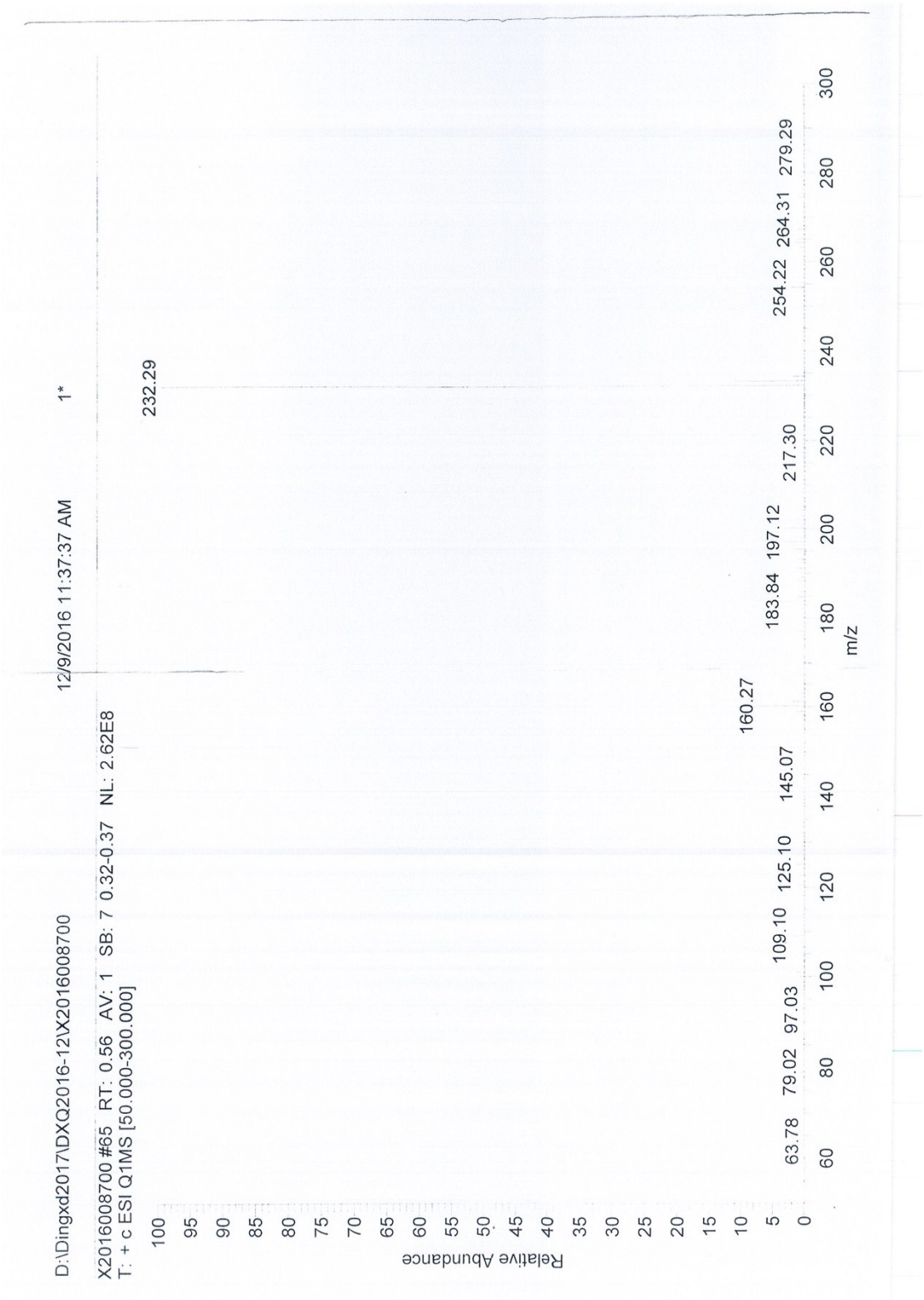

Figure S3. ESI-MS spectrum of intermediate product.

ESI-MS ($C_{14}H_{18}O_2N$ (calculated at 232.3): m/z 232.3.

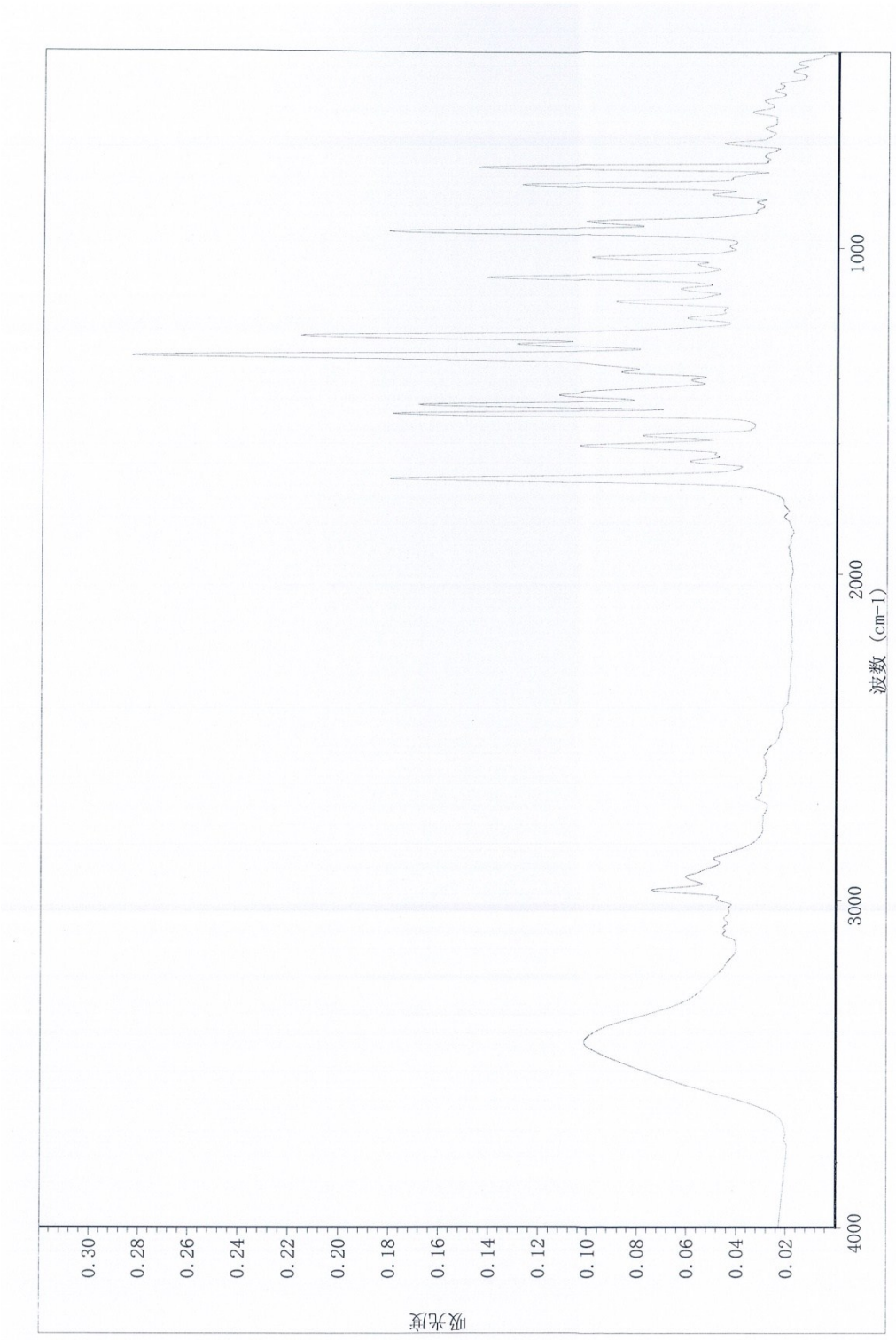

Figure S4. FTIR spectrum of SP.

FTIR (4000-400, cm^{-1}): dominated absorbance peaks, 1710 (υ_{COOH}), 1611 ($\upsilon_{C=C}$), 1332, 1509 ($\upsilon_{Ar\text{-}NO2}$), 1272, 1028 ($\upsilon_{C\text{-}O\text{-}C}$).

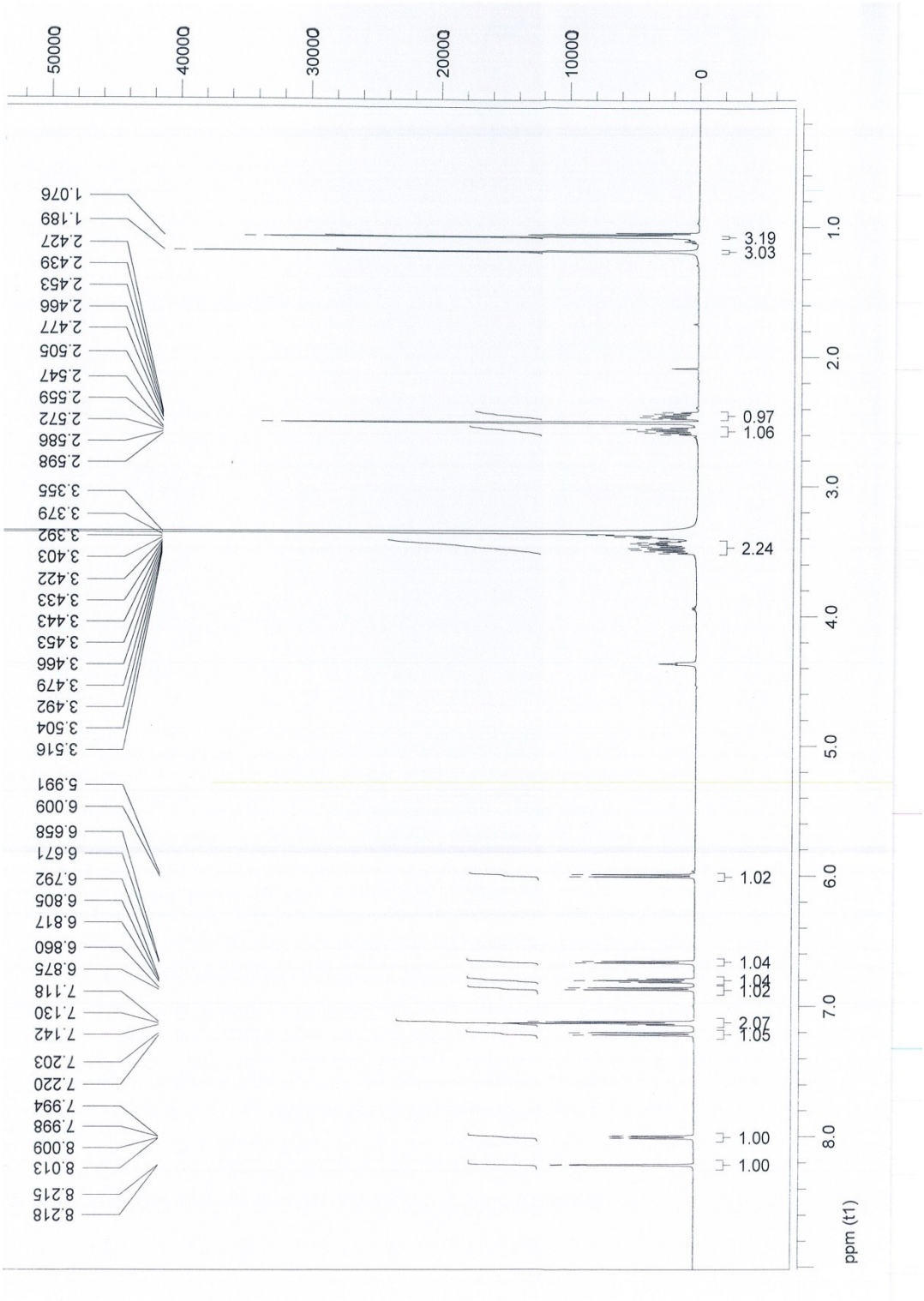

Figure S5. ^{1}H NMR spectrum of SP.

^{1}H NMR (DMSO-d_6, 600 MHz): δ 1.07 (s, 3H), δ 1.19 (s, 3H), δ 2.43-2.59 (m, 2H), δ 3.35-3.52 (m, 2H), δ 5.98-6.01 (d, 1H), δ 6.65-6.67 (d, 1H), δ 6.79-6.81 (t, 1H), δ 6.85-6.87 (d, 1H), δ 7.11-7.14 (t, 2H), δ 7.20-7.21 (d, 1H), δ7.99- 8.01 (dd, 1H), δ 8.21 (d, 1H).

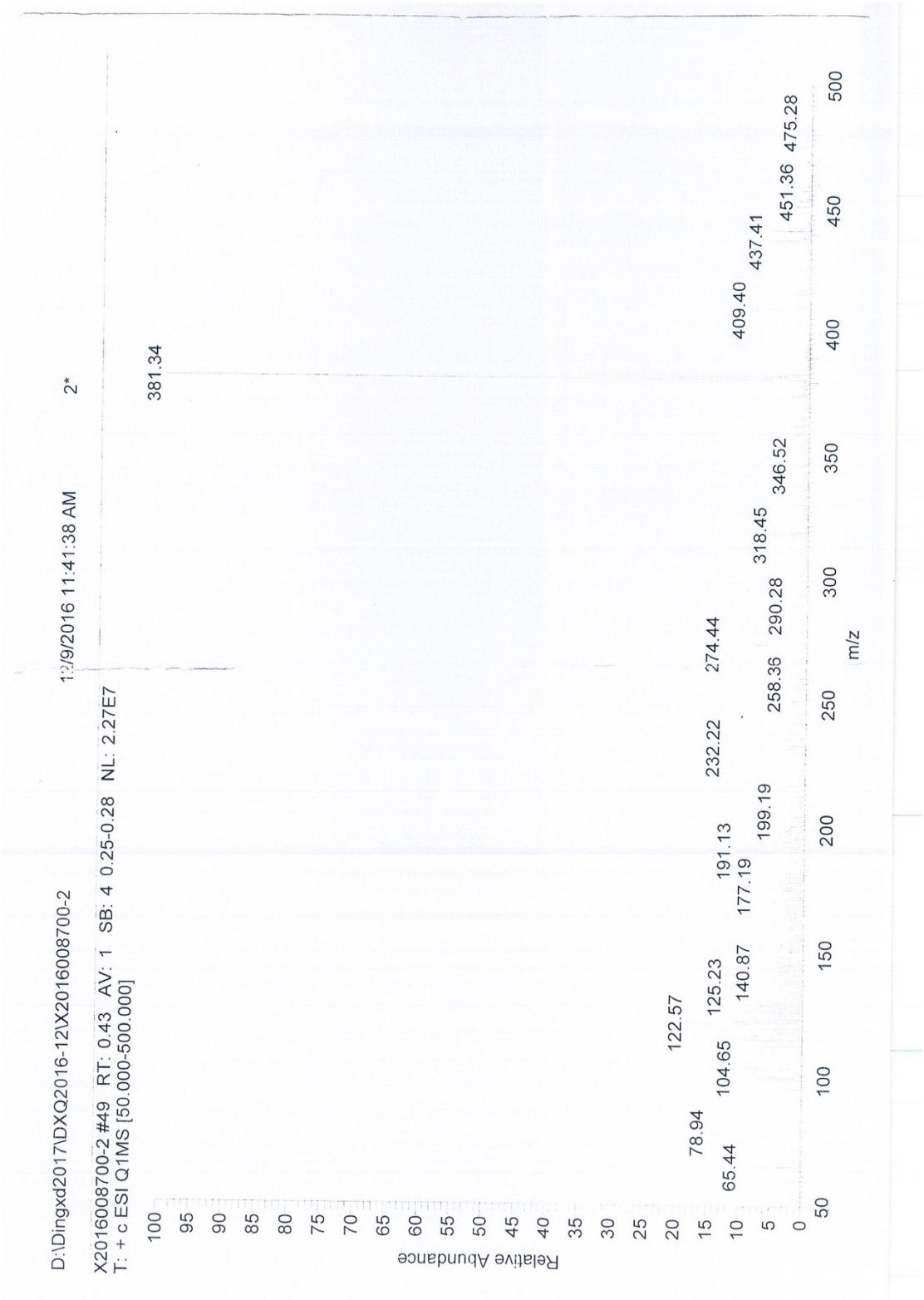

Figure S6. ESI-MS spectrum of SP.

ESI-MS ($C_{21}H_{20}O_5N_2$ (calculated at 380.4): m/z 381.3 ($M+H^+$).

4.2 Photostationary states of spiropyran

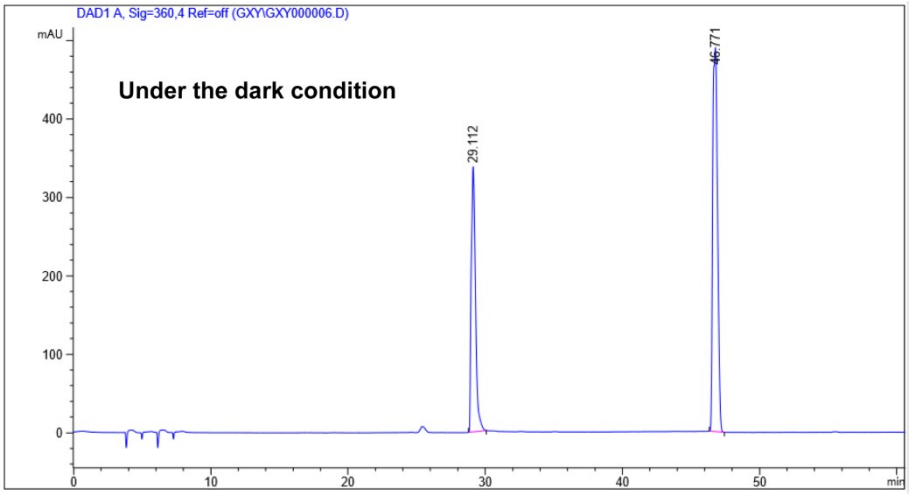

<Peak table>

Peak#	Ret.Time	Area%
1	29.112	37.794
2	46.771	62.206
Total		100.000

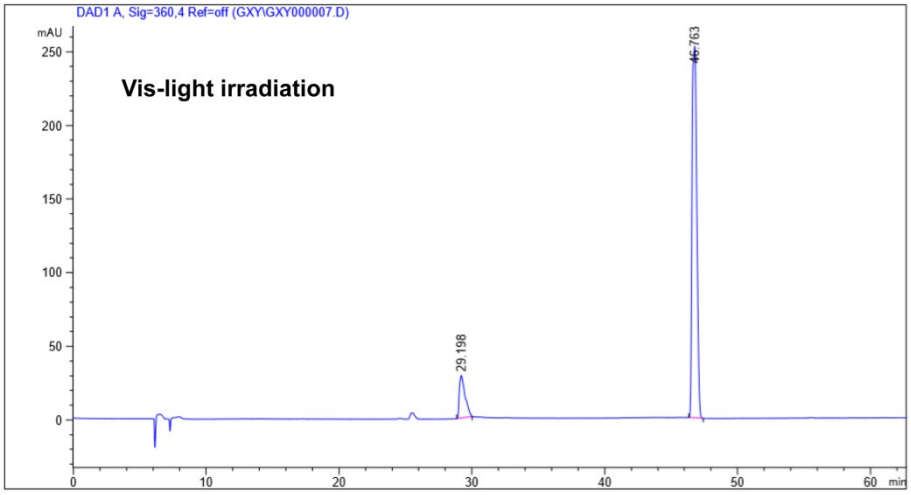

<Peak table>

Peak#	Ret.Time	Area%
1	29.198	12.431
2	46.763	87.569
Total		100.000

Figure. S7 SP:MC ratio of spiropyran (2.5×10^{-4} M) in DMF/H_2O solution (50:50 v/v, 293 K) under the dark condition for 240 min and after visible light irradiation for 20 min, determined by HPLC.

4.3 Job's and Benesi-Hildebrand plot of MC with Cr(III)

In order to determine complex-ratio between MC and Cr(III), the composition of the complex was analyzed spectrophotometrically *via* the isomolar solution technology (Job's method of continuous variation), successfully applying in the analysis of the other spirochromene metal complex [3]. As could be seen in Figure 1(c) (Main manuscript), a plot that the absorbance value measured at the adsorption maximum (420 nm) of the complex MC-Cr(III) versus the Cr(III) molar ratio of isomolar solutions, the apex was located at a Cr(III) molar ratio of 0.45, corresponding to a MC-Cr(III) approximate stoichiometry of 1:1. Moreover, the binding constant k of MC-Cr(III) could be further calculated based on Benesi-Hildebrand equation [4]:

$$\frac{1}{A_x\text{-}A_0} = \frac{1}{k(A_{\max} - A_0)[Cr(III)]} + \frac{1}{A_{\max} - A_0} \qquad \text{(S1)}$$

Where A_0, A_x, and A_{max} are the UV-Vis absorption intensities of the MC-Cr(III) complex at 420 nm considered in the absence of Cr(III), at a certain concentration of Cr(III), and with an excess amount of Cr(III), respectively; k is the binding constant and [*Cr(III)*] is the concentration of Cr(III). The k value of 0.53×10^4 M^{-1} was extrapolated from the slope of the plot $(A_{max}\text{-}A_x)/(A_x\text{-}A_0)$ against 1/[*Cr(III)*] (Figure 1(d), Main manuscript). On the other hand, the plot of $(A_{max}\text{-}A_x)/(A_x\text{-}A_0)$ against 1/[*Cr(III)*] shown a liner relationship, further indicating that MC indeed associated with Cr(III) in a 1:1 stoichiometry.

4.4 MC→SP and MC-Cr(III)→SP(Cr(III)) transition by visible light irradiation

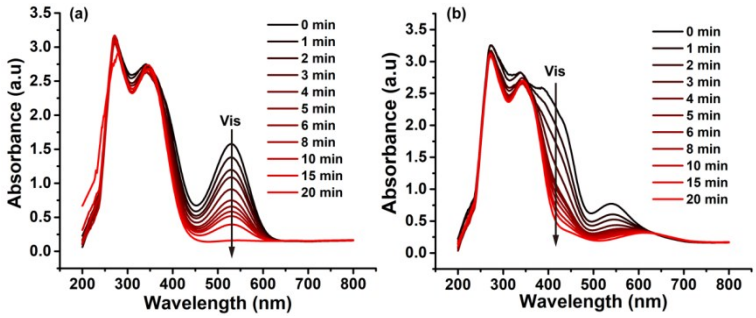

Figure S8. UV-Vis absorbance spectra of (a) SP (2.5×10^{-4} M) in DMF/H_2O solution (50:50 v/v, 293 K) and (b) after addition of 1 equivalent Cr(III) with visible light irradiation over time.

4.5 Morphology of freshly cleaned SW

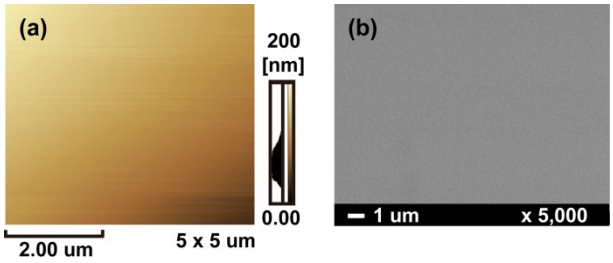

Figure S9. AFM (a) and SEM (b) images of cleaned SW.

4.6 Fluorescence emission spectra of SP and MC

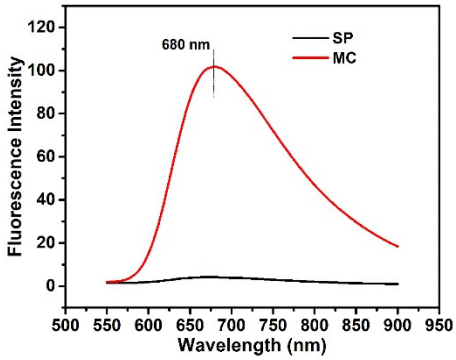

Figure S10. Fluorescence emission spectra (λ_{ex} = 360 nm) of SP (2.5 × 10^{-4} M) and MC in DMF/H_2O solution (50:50 v/v, 293 K). The closed spiro-form (SP) did not exhibit an emission, while the zwitterionic mero-form (MC) was appearance an intense emission band centered at λ_{max} ≈ 680 nm. 680 nm is in the range of red light (approximate from 620 to 750 nm).

4.7 Morphology of naked Fe_3O_4

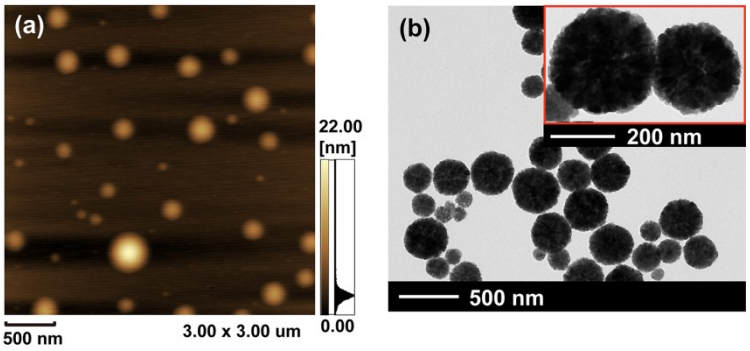

Figure S11. AFM (a) and TEM (b) images of naked Fe_3O_4. AFM and TEM images indicated that naked Fe_3O_4 was spherical with an approximate diameter of 280 nm.

4.8 Characterization of SP@Fe_3O_4

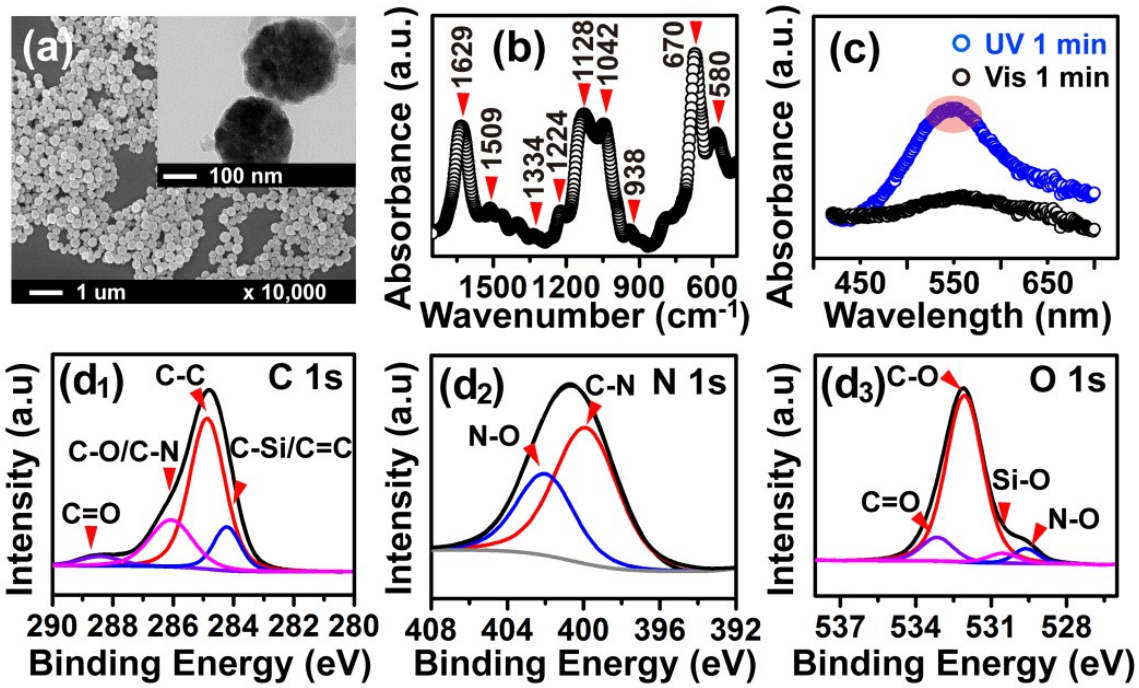

Figure S12. (a) SEM image (inset is the TEM image), (b) FTIR spectrum, (c) UV-Vis absorbance spectra, and (d_1) C 1s, (d_2) N 1s and (d_3) O 1s high-resolution XPS spectral envelopes of SP@Fe_3O_4. To separate different species of the same element, CasaXPS processing software was employed to deconvolve the XPS signals with Gaussian-Lorentzian function (Gaussian=80%, Lorentzian=20%) after subtraction of a Shirley background. Compared with the naked Fe_3O_4 shown in Fig. S11, a layer of light contrast could be visualized around the particles which were displayed as dark contrast. In FTIR spectrum, peaks at 1629, 1334, 1224, and 938 cm^{-1} were ascribed to C=C, Ar-NO_2, C-O-O, and Ar-N groups of SP moieties, respectively. The peak at 1509 cm^{-1} was associated with the amide II stemming from amide couplings between amine terminals from AMEO and the activated carboxyl in SP. Furthermore, peaks at 1128, 1042 and 670 cm^{-1} were stirred from AMEO Si-O-Si group, while 580 cm^{-1} was Fe-O signal derived from Fe_3O_4. UV-Vis absorbance spectra of SP@Fe_3O_4 demonstrated that SP was successfully conjugated onto Fe_3O_4 surface, thus shown sensitive to light stimulation. XPS spectral envelopes of SP@Fe_3O_4 further indicated the success of synthesis.

4.9 Effect of initial Cr (III) concentration on Cr adsorption by adsorbents

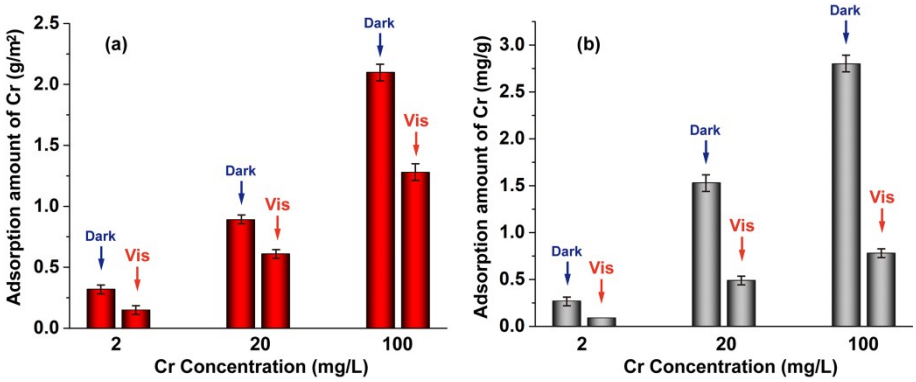

Figure S13. Adsorption amount of Cr by SP@SW (a) and SP@Fe_3O_4 (b) upon alternating visible light irradiation (30 min) and under the dark (4 h) condition with different initial Cr (III) concentration.

Industrial sources of chromium include leather tanning, cooling tower blowdown, plating, electroplating, anodizing baths, rinse waters, *etc*. The concentrations of their discharged chromium-contaminated water range from a few to hundred milligrams per liter. In this work, three different concentrations of Cr (III)-contaminated water, *i.e.*, 2, 20, and 100 mg/L, were investigated. Considering universality of present designed adsorbents (SP@Fe_3O_4 and SP@SW) to more fields, moderate concentration (20 mg/L) of Cr (III) water was chosen for the following experiments.

4.10 Effect of visible light irradiation time on Cr desorption from adsorbents

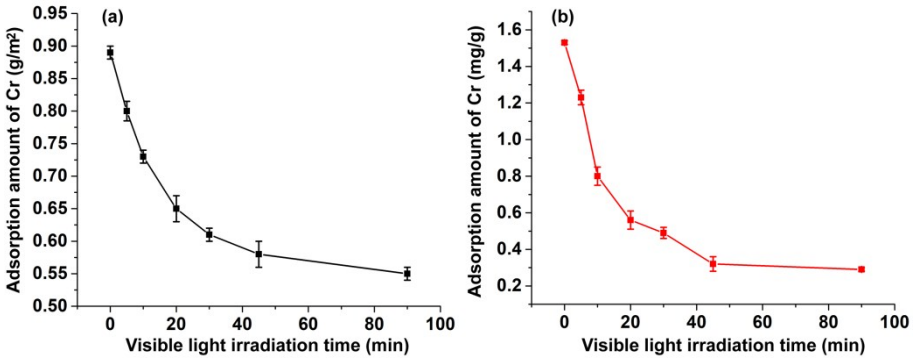

Figure S14. Adsorption amount of Cr by SP@SW (a) and SP@Fe3O4 (b) with increasing visible light irradiation time.

Comprehensive consideration of enhancing Cr-desorbed potency by visible light stimulus and reducing of photodegradation of the adsorbents (increasing irradiation time accelerating photodegradation), visible light irradiation for 30 min was selected for all desorption experiments.

4.11 Adsorption potency of different metal ions (M^{n+}) by SP@Fe_3O_4

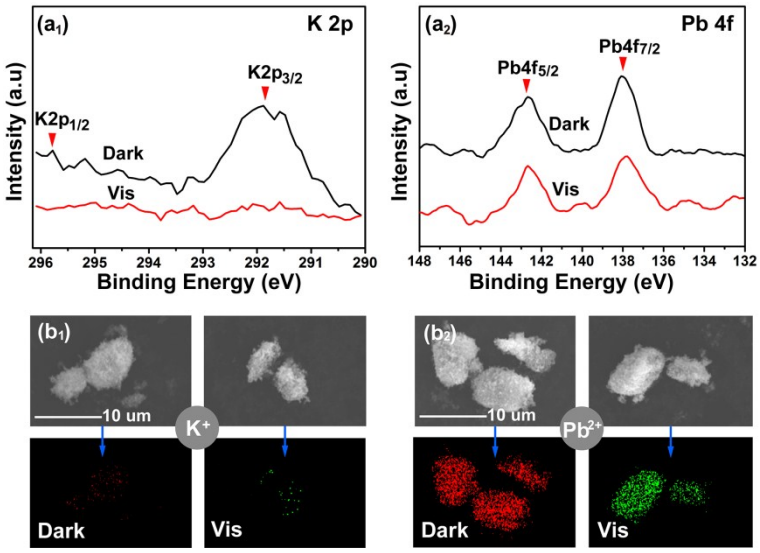

Figure S15. High resolution of (a_1) K 2p, (a_2) Pb 4f XPS spectra, and zero-loss SEM images and corresponding EDS K-mapping (b_1) and Pb-mapping (b_2) of SP@Fe_3O_4 after K^+ and Pb^{2+} triggering under the dark and visible light (Vis) irradiation condition.

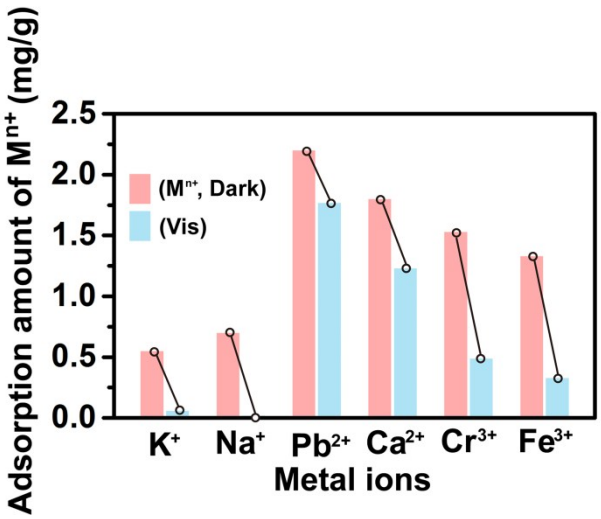

Figure S16. Adsorption amount of different metal ions by SP@Fe_3O_4 under the dark and visible light (Vis) illumination.

In order to evaluate the binding capacity of present designed adsorbents to other metal ions (M^{n+}), five M^{n+} with different valence, *i.e.*, K^+, Na^+, Pb^{2+}, Ca^{2+}, and Fe^{3+}, were employed, and the experimental condition was same to that of Cr^{3+}. Herein, take

SP@Fe_3O_4 for the target adsorbent. Furthermore, SP@Fe_3O_4 composites interacted by the representative metal ions with different chemical valence (K^+, Pb^{2+}, and Cr^{3+}) were selected for qualitative analysis of M^{n+} coordination and dissociation. As could be seen in Fig. S15 (b) and Fig. 3 (b_2) , EDS mapping of K^+ (Fig. S15, b_1), Pb^{2+} (Fig. S15, b_2), and Cr^{3+} (Fig. 3 (b_2)) elements under dark condition (distribution with red color) demonstrated that SP@Fe_3O_4 had a coordination ability to different valent metal ions, but showed variable induction strength to them. The phenoxide anions in SP moiety presented the highest affinity binding to Pb^{2+} manifested by a dense distribution of it on the exhausted SP@Fe_3O_4, while demonstrated the lowest to K^+ and centered to Cr^{3+}. Furthermore, after regeneration of SP@Fe_3O_4 by visible light irradiation, those coordinated M^{n+} were dissociated partly, but still remained on the composites surface (distribution with green color). The relative amount of M^{n+} released from the composites by Vis-light stimulation can't get exactly only by EDS technology. Meanwhile, high resolution of K 2p, Pb 4f, and Cr 2p XPS spectra of the exhausted and regenerated SP@Fe_3O_4 (see Fig. S15 (a) and Fig. 3 (c_2)) produced similar results with those of EDS mapping. For the purpose of quantitative analysis of M^{n+} coordinated and dissociated by SP@Fe_3O_4, respectively, the residual concentration of them was also determined by ICP-OES and the results were presented as a histogram in Fig. S16. Indeed, the SP moiety in SP@Fe_3O_4 structure had strong coordination ability to divalent metal ions (M^{2+}), such as Pb^{2+} and Ca^{2+}, because of the low Gibbs free energy (ΔG) of the interaction between the MC and M^{2+} (-239.5 kcal/mol for Pb^{2+}, -162.7 kcal/mol for Ca^{2+}, obtained by using density functional theory (DFT) [1]). Theoretically, a negative value of ΔG indicates a spontaneity and feasibility of such binding process, while ΔG are lower, the interaction force between MC and M^{n+} are stronger. In spite of the strong binding capacity of SP moiety to M^{2+} facilitating them removal from water, it was difficult to release M^{2+} thus regenerate SP@Fe_3O_4 composite only by Vis-light stimulus. As for the monovalent metal ions, K^+ and Na^+, the phenolate group in SP moiety showed low combining capacity with them, but those combined M^+ were easy to dissociate from the composite. Based on the previous reports [5-7], M^+ sensing or binding scarcely employed SP molecular, while other photosensitive compounds

containing crown ether structure, such as azobenzenes [5], diarylethenes [6], and fulgides [7], were favor to select for studying their interaction processes. Additionally, coincident with the EDS mapping results, the coordination and dissociation capacity of SP@Fe_3O_4 to trivalent metal ions (M^{3+}) were centered, which corresponded to the larger ΔG of the interaction between the MC and M^{3+} (-68.2 kcal/mol for Cr^{3+}, and -49.5 kcal/mol for Fe^{3+} [1]). It was worth nothing, however, that the relative amount of M^{3+} released from their composites by Vis-light irradiation was the largest compared with those of M^{+} and M^{2+}, indicating that efficient light-driven composite-regeneration was achieved with moderately stable complexes, rather than with unstable (M^{+}[MC-moiety]) or very stable complexes (M^{2+}[MC-moiety]). Based on these, SP@Fe_3O_4 could potentially be used as an adsorbent for M^{n+}. Moreover, on account of adsorption/desorption requirement; this adsorbent will be propitious to various metal ions with different chemical valence. For example, if it needs high adsorption capacity but has no request for regeneration of the adsorbent, SP@Fe_3O_4 fits to M^{2+}, such as Pb^{2+}. Besides, partial M^{3+}, exemplified by Cr^{3+}, will be selected in case of the photosensitive desorption method being necessary rather than chemical desorption (by acid or alkaline substance). Nevertheless, SP@Fe_3O_4 is not suitable for monovalent metal ions due to low adsorption ability to them.

4.12 Three cycles of Cr(III) adsorption by SP@SW and SP@Fe_3O_4

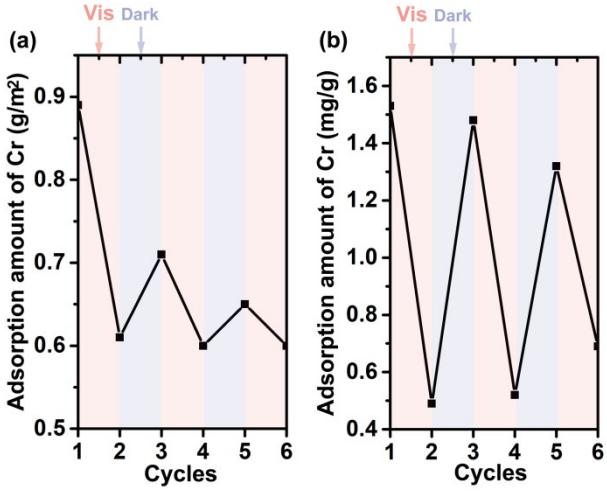

Figure S17. Three cycles of Cr (III) adsorption by SP@SW (a) and SP@Fe_3O_4 (b) upon alternating visible light irradiation (30 min) and under the dark (4 h) condition.

4.13 Fatigue analysis of MC and MC-Cr(III) moving around freely in solution

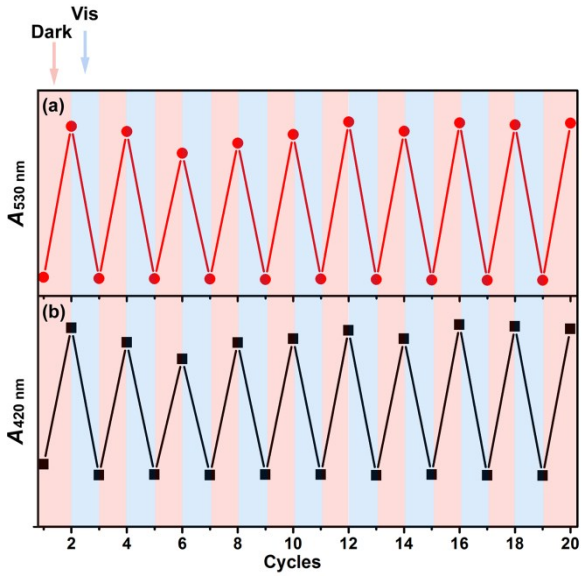

Figure S18. Sequential cycles of conversion between (a) SP (2.5×10^{-4} M) and MC, (b) SP/Cr(III) ($2.5/2.5 \times 10^{-4}$ M) and MC-Cr(III) controlled by visible light (irradiation for 30 min) and dark (placing for 4 h) condition in DMF/H_2O solution (50:50 v/v, 293 K).

References

[1] Dingbin Liu, Wenwen Chen, Kang Sun, Ke Deng, Wei Zhang, Zhuo Wang, and Xingyu Jiang. Resettable, multi-readout logic gates based on controllably reversible aggregation of gold nanoparticles. Angewandte Chemie International Edition. 2011, 50(18), 4103-4107.

[2] Hong Deng, Xiaolin Li, Qing Peng, Xun Wang, Jinping Chen, and Yadong Li. Monodisperse magnetic single-crystal ferrite microspheres. Angewandte Chemie. 2005, 117, 2842−2845.

[3] Manuel Natali, Laura Soldi, Silvia Giordani. A photoswitchable Zn (II) selective spiropyran-based sensor. Tetrahedron, 2010, 66, 7612-7617.

[4] Manuel Natali, Christer Aakeröy, ohn Desper and Silvia Giordani. The role of metal ions and counterions in the switching behavior of a carboxylic acid functionalized spiropyran. DaltonTransactions. 2010, 39, 8269–8277.

[5] Seiji Shinkai, Kazuyoshi Shigematsu, Michiko Sato and Osamu Manabe. Photoresponsive crown ethers. Part 6. Ion transport mediated by photoinduced cis—trans interconversion of azobis (benzocrown ethers). Journal of the Chemical Society, Perkin Transactions. 1982, 1, 2735-2739.

[6] Michinori Takeshita, Masahiro Irie. Photoresponsive tweezers for alkali metal ions. Photochromic diarylethenes having two crown ether moieties. The Journal of Organic Chemistry. 1998, 63, 6643-6649.

[7] Yasushi Yokoyama, Takabumi Ohmori, Tomoyuki Okuyama, Yayoi Yokoyama, Soichi Uchida. Photochromism of fulgenates possessing crown-ether moiety. Molecular Crystals and Liquid Crystals Science and Technology. Section A. Molecular Crystals and Liquid Crystals. 2000, 344, 265-270.